Research Article | Vol. 9, No. 10 / 1 October 2019 / Optical Materials Express 3968
Optical Materials EXPRESS

Bio-inspired materials as interfacial layers for high performance perovskite photodetectors

ZHAN GAO,[1,2] XINYU ZHANG,[1] JUNSHENG YU,[1,3] AND XINGE YU[2,4]

[1]State Key Laboratory of Electronic Thin Films and Integrated Devices, School of Optoelectronic Science and Engineering, University of Electronic Science and Technology of China (UESTC), Chengdu 610054, China
[2]Department of Biomedical Engineering, City University of Hong Kong, Hong Kong, China
[3]jsyu@uestc.edu.cn
[4]xingeyu@cityu.edu.hk

Abstract: Perovskites have shown potential for use as high performance photodetectors, where the responsivity and detectivity of the perovskite photodetector (PePDs) can be improved by engineering its interfacial properties. Herein we report the applications of bio-inspired materials, deoxyribonucleic acid (DNA) and guanine, as functional interfacial layers for high performance PePDs. The best bio-material modified PePDs exhibit a ~2× enhancement of the photo-current than that of the reference PePDs with no modifications. Further optimization of the thickness for the bio-materials based functional layers enables the PePD to achieve a remarkable responsivity of 0.37 A W^{-1} and detectivity of 1.85×10^{12} Jones at the wavelength of 745 nm. Electrical and morphological studies of the PePDs indicate that DNA functional layers acting as electron extraction pathways could effectively enhance the photo-current. Our work comes up with an ecofriendly and low-cost method for fabricating high performance PePDs and therefore provides foundations for the future exploration of the application of bio-materials in opto-electronics.

© 2019 Optical Society of America under the terms of the OSA Open Access Publishing Agreement

1. Introduction

Recently, organic-inorganic hybrid perovskites have received enormous interest due to their great optoelectronic properties [1–10]. Multiple advantages in perovskites, such as remarkable light absorption, tailorable absorption spectra, and high charge carrier mobility have made perovskites promising candidates for high performance photodetectors [11]. In 2014, Hu et al. for the first time reported perovskites photodetectors (PePDs), with a broad optical absorption range that associated with a photo-responsivity of 0.0367 A W^{-1} and 3.49 A W^{-1} at 365 nm and 780 nm, respectively [12]. Since then, various strategies have been adopted to enhance the performance of PePDs in recent years, among which the optimal responsivity is over 10^9 A W^{-1} [13]. Despite of these promising results, however, there are still great room for further improvement of the light harvesting efficiency in PePDs, according to the inherent optoelectronic properties of perovskite materials.

In general, the light harvesting efficiency of PePDs is strongly related to the extraction and transport of the photo-induced charge carriers. The existing of defects at the interfaces, energy-level mismatch between perovskites and metal electrodes and carrier traps could restrict the transport of charge carriers, thus degrade the device performance [11,14]. Many research works focusing on interfacial engineering have been conducted for improving the interfacial properties in PePDs. For instance, using perovskite: PbS quantum dots (QDs) for enhancing the built-in potential between perovskites and PbS QDs can efficiently drive the separation of photo-generated charge carriers, and therefore resulting in enhanced detectivity [15,16]. Another successful interfacial engineering for PePDs is utilizing certain materials with high charge carrier mobility such as graphene and WS_2 as interfacial layers to assist the interfacial charges separation [17–19]. Nevertheless, the development of the abovementioned functional materials either require long

#374142 https://doi.org/10.1364/OME.9.003968
Journal © 2019 Received 30 Jul 2019; revised 30 Aug 2019; accepted 30 Aug 2019; published 6 Sep 2019

Optical Materials EXPRESS

processing period, or have the hazardous risk, which limited large-scale fabrications and practical applications. Therefore, it is desirable to exploit low-cost and ecofriendly materials as functional interfacial layers for high performance PePDs. With rapid development of optoelectronics, interdisciplinary concepts of bio-integrated and bio-inspired electronics have attracted great of attentions in recent years, where bio-inspired and bio-compatible materials arises as natural candidates [20–26]. Overviewing bio-materials that reported in the literatures, deoxyribonucleic acid (DNA) is recognized as a unique one, as which can act as charge injection layers, electron blocking layers and dielectric layers in optoelectronic devices [27–36]. For example, Zalar et al. adopted DNA as a functional layer for electron injection and hole blocking in polymer light-emitting diodes, and therefore achieved great device performance [28]. Dagar et al. introduced DNA as an electron-extracting layer in polymer solar cells, and successfully improved rectifying behavior and power conversion efficiencies [32]. These results indicate the great potential of bio-materials for the fabrication of high-performance optoelectronics.

In this work, we for the first time report ecofriendly and low-cost bio-materials, DNA and guanine as interfacial layers to modify the perovskite film in PePDs. Compared with that of the bare perovskite layered photodetectors, the DNA and guanine modified PePDs exhibit a remarkable enhancement of photo-current from 1.66×10^{-4} A to 3.08×10^{-4} A and 2.48×10^{-4} A at −0.2 V, respectively. Furthermore, we optimized the thickness of the DNA interfacial layers and obtained a high-efficient PePD with a high responsivity of 0.37 A W^{-1} and a high detectivity of 1.85×10^{12} Jones at the wavelength of 745 nm. By analyzing the morphology of the perovskite film and the impedance of the PePDs, we found that DNA acts as electron-extracting pathways and thus promotes the photo-current of the device.

2. Method

The perovskite precursor solution was prepared by mixing 744 mg CH_3NH_3I (MAI) with 254.3 mg PbI_2 (Polymer Light Technology Corp.) in 1 mL N,N-Dimethylformamide (Sigma-Aldrich). The fabrication process began on ITO coated glass substrates where the thin film ITO with a sheet resistance of 15 Ω/sq served as anodes. The substrates were cleaned in an ultrasonic bath with detergent water, acetone, deionized water, and isopropyl alcohol for 15 min each sequentially. Then the ITO glasses were nitrogen blew dry and treated by oxygen plasma under a pressure of 25 Pa for 5 min to modify the surface energy. PEDOT:PSS was spin-coated at 5000 rpm for 60 s and immediately annealed at 145°C on a hotplate for 15 min. After the cleaning and surface treatment, substrates were transferred into a N_2 filled glove box for the next step. The perovskite solution was spin-coated onto the PEDOT:PSS film (2500 rpm for 40 s). 300 μL chloro-benzene (CB) was dropped onto the samples during spin-coating. Samples were then annealed at 105°C for 15 min. Guanine (Sigma-Aldrich) were dispersed in CB with a concentration of 0.5 mg/ml. Deoxyribonucleic acid (DNA) extracted from fish sperms (Sigma-Aldrich) were dispersed in CB forming various concentrations from 0.5 wt. % to 2.5 wt. %. The solution was spun at 5000 rpm for 40 s on the perovskite film and annealed at 100 °C for 10 min. Afterwards, $PC_{61}BM$ dissolved in dichlorobenzene (18 mg/ml) was spun at 3000 rpm for 40 s and annealed at 100 °C for 20 min. Since the solubility of DNA in dichlorobenzene is very poor, spin-coating $PC_{61}BM$ on top wouldn't damage the DNA interfacial layer. Finally, 100 nm thick Ag serving cathodes were vacuum deposited onto the film under 10^{-5} mbar. The overlap between ITO and Ag electrodes of 0.02 cm^2 act as the active absorption area.

The current density-voltage-luminance (*J-V-L*) characteristics were tested in dark room with a white light source (100 mW/cm^2) by a Keithley 4200 source. The absorption spectra were performed by a Horiba 320 detector. The surface morphologies were measured by a top-view scanning electron microscopy (FEI Inspect F50). The micro structures and crystallinity were analyzed by X-ray diffraction spectrometry (D2 PHASER). The impedance measurements were conducted by a precision impedance analyzer (Agilent 4294A).

Optical Materials EXPRESS

3. Result

Figure 1(a) shows the schematic diagram of the PePD devices used in this work, where the multiple layers structure consists of indium tin oxide (ITO), poly(3,4-ethylenedioxythiophene):polystyrene sulfonate (PEDOT:PSS) (40 nm), $MAPbI_3$ (~400 nm), DNA or Guanine, $PC_{61}BM$ (70 nm), and Ag (~100 nm). Bio-materials DNA and guanine serving as the interfacial layers were selected for modifying the perovskite thin film, due to the following reasons. Firstly, these two materials are low-cost, as $3/g for DNA and Guanine, which is over 400× cheaper than the widely reported interfacial materials, such as graphene ($1345/g, Sigma Aldrich). Secondly, they are also bio-compatible and ecofriendly materials, thus owning potentials for next generation bio-integrated photonics. Thirdly, the inherent of nano features of these materials facile the charge carrier injection and extraction, such that evidences have been proven in organic electronics [27–33]. To investigate the roles of the DNA and guanine interfacial layers on the device performance, photocurrent (I_{ph}) and dark current (I_d) of the PePDs were tested under white light (100 mW/cm^2) irradiation and dark condition, respectively. Figure 2(a) summarizes the I_{ph} as a function of operating voltages for the PePDs without bio-materials and with bio-materials modification, where the reference PePDs without bio-materials show a low I_{ph} of 1.66×10^{-4} A at a bis of −0.2 V, and the bio-materials modified PePDs exhibit an enhanced I_{ph} of 2.27×10^{-4} A for guanine modified devices and 3.09×10^{-4} A for DNA modified devices. These results clearly show that the introduction of bio-materials based interfacial layers could effectively enhance the device performance, since great I_{ph} is an essential factor for high-performance PePDs. Another two key factors for PePDs are high detectivity (D^*) and low I_d. As shown in Fig. 2(b), the PePDs with guanine and DNA exhibit I_d of 1.06×10^{-7} A and 9.33×10^{-8} A at bias of −0.2 V, respectively, which maintain the similar value that of the reference PePDs.

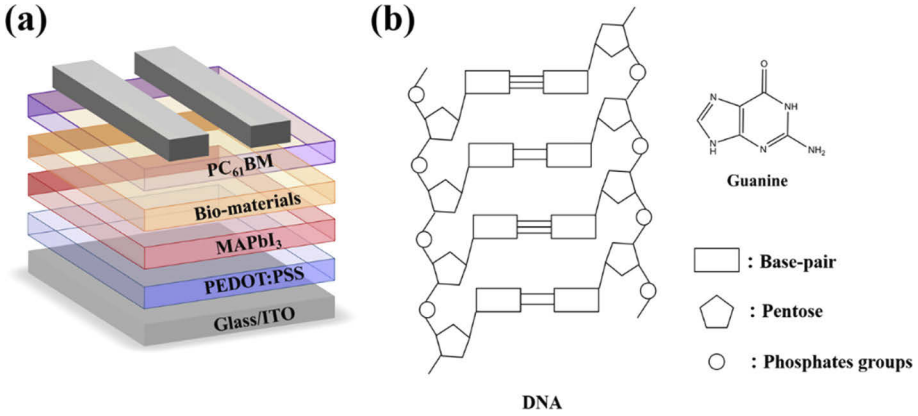

Fig. 1. (a) The schematic diagram of the PePD, where the bio-materials used as interfacial layers; (b) Molecular structures of the bio-materials: deoxyribonucleic acid (DNA) and guanine.

The great I_{ph} and I_d in the DNA modified PePDs suggest that DNA is a promising candidate interfacial material for high performance PePDs. Next, further optimization of the device performance via investigating the concentration for DNA solution was conducted. Figure 2(c) shows the J-V curves of PePDs with different thickness of the DNA interfacial layer that spun-casted with various solution concentrations of 0.5 wt.%–2.5 wt.%. PePDs with 0.5 wt.%, 1.5 wt.% and 2.5 wt.% DNA show I_{ph} values of 3.09×10^{-4} A, 3.84×10^{-4} A and 2.25×10^{-4} A, at bias of −0.2 V, respectively. Increasing the concentrations of the DNA solution from 0.5 wt.% to 1.5 wt.% leaded to a slight enhancement of I_{ph}. While further increase the concentration of DNA to 2.5 wt.% caused a deteriorate of I_{ph}. These results indicate that high concentration of

Optical Materials EXPRESS

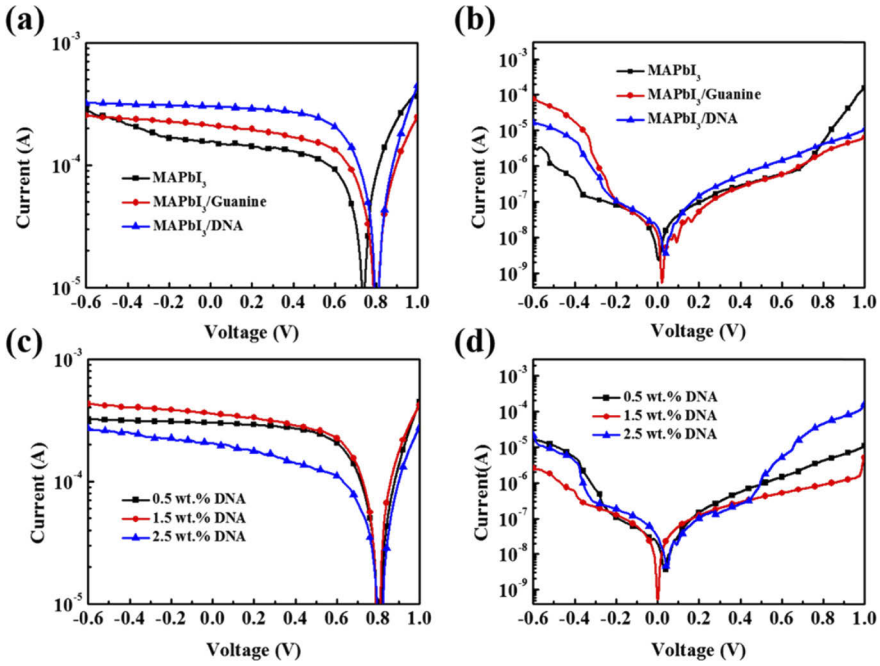

Fig. 2. Semi-log J-V characteristics of PePDs with and without bio-materials under light (a) and (b) dark condition. Semi-log J-V characteristics of PePDs with various concentration of DNA under light (c) and dark (d) condition.

DNA could hinder the extraction of photon-generated charge carriers [15]. *J-V* characteristics measured under dark condition show the I_d of 9.33×10^{-8} A for 0.5 wt.%, 1.26×10^{-7} A for 1.5 wt.% and 1.84×10^{-7} A for 2.5 wt.% DNA solution formed devices.

To investigate the photonic properties of these PePDs, the external quantum efficiencies (EQEs) of the PePDs were measured and analyzed. Figure 3(a) presents the measured EQE spectra of the PePDs with different concentrations of DNA. The EQE for the control device is relatively low compared to the devices with 0.5 wt.% and 1.5 wt.% DNA. The EQE for the PePD with 1.5 wt.% DNA exhibit the greatest photo-gain in the region between 500 nm and 800 nm. Interestingly, higher DNA concentration of 2.5 wt.% results in a dramatically decrease of EQE, which is consistent with the results of I_{ph}. The responsivity (R) is typically used for determining the conversion ratio from photons to charge carriers, that can be calculated by the following equation:

$$R(\lambda) = \frac{J_{ph}}{L_{light}} = EQE(\lambda)\frac{\lambda q}{hc} \tag{1}$$

where q is the electron charge, λ is the wavelength, h is the Planck constant, c is the light velocity, and L light is the incident light intensity [37]. The trend of R highly depends on the EQE. As shown in Fig. 3(b), the highest R among all devices is the PePD with 1.5 wt.% DNA, which is 0.37 A W^{-1} at the wavelength of 745 nm. Another important parameter for PePDs – D^*, is used to characterize the photo sensitivity of the devices, which can be calculated using the following equation:

$$D^*(\lambda) = \frac{R(\lambda)}{\sqrt{2q \times J_d}} \tag{2}$$

where J_d is dark current density. From *Eq.* (2), it is obvious that higher R and lower J_d are desirable for higher D^*. The calculated D^* for these PePDs at −0.2 V are summarized in Fig. 3(c)

Optical Materials EXPRESS

and Table 1. The device with 1.5 wt.% DNA exhibits the highest values of D^* over the entire viable spectral range and reaches 1.85×10^{12} Jones at the wavelength of 745 nm. The remarkable D^* for this kind of devices basically attributes to the enhancement of I_{ph}. Figure 3(d) shows the dynamic measurement of the photo response in PePDs as a function of time, where it can be found the photo responsivity of the PePDs for both reference devices and devices with DNA interfacial layers reveal rapid photo response. The current of these PePDs increased immediately as the light irradiation was introduced, and decreased to its original level once light off. As shown in Fig. 3(e), the response of I_{ph} in the PePD with DNA interfacial layers is more intense and faster than the reference devices, indicating the efficient charge separation at the interface is consistent and repeatable [19,38]. In addition, the I_{ph} of the control device in the fourth period is smaller than its initial value. The reduction of photocurrent is due to the performance degradation caused by water molecular and oxygen, as the photo-response measurements were conducted under ambient condition without encapsulation [14].

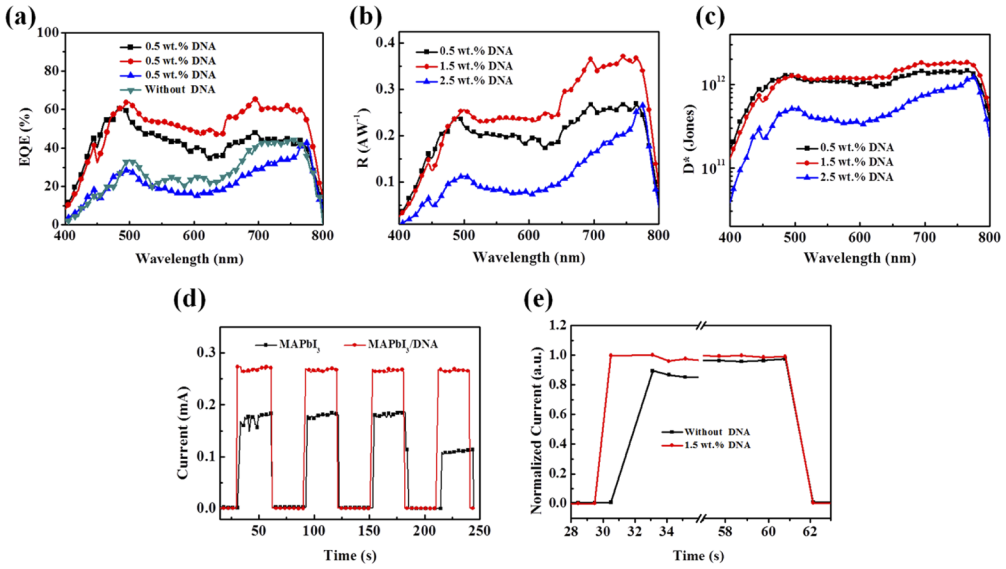

Fig. 3. Electrical properties of interfacial layer modified PePDs with spun-cast various concentrations of DNA. Measured EQE spectra (a), calculated R* values at −0.2 V (b), and calculated D* values at −0.2 V (c) for PePDs at wavelength from 400 nm to 800 nm. (d) Dynamic photo response measurements of two kinds of PePDs by multiple cycles introducing and removal light (intensity of 100 mW/cm^2) (e) Temporal photo-response of the PePDs with 1.5 wt.% DNA and without DNA.

Table 1. Summary of the electrical properties, I_d, I_{ph} and R for various kinds of PePDs at −0.2 V; D^* for all devices were measured at 745 nm.

Devices	I_d ($\times 10^{-8}$A)	I_{ph} ($\times 10^{-4}$A)	R (A W^{-1})	D^* ($\times 10^{12}$Jones)
0.5 wt.% DNA	9.33 ± 0.11	3.09 ± 0.15	0.26 ± 0.01	1.45 ± 0.01
1.5 wt.% DNA	1.26 ± 0.17	3.84 ± 0.11	0.37 ± 0.02	1.85 ± 0.02
2.5 wt.% DNA	1.84 ± 0.21	2.25 ± 0.16	0.20 ± 0.01	9.21 ± 0.02

UV-Vis absorption spectra for the PePDs with and without DNA interfacial layers were measured as shown in Fig. 4(a), from which it can be seen the absorption spectra of these two films are almost overlap. This result indicates that thin DNA interfacial layer doesn't change the light absorption properties in visible range of the perovskite films. Then the mirco structures

Optical Materials EXPRESS

the perovskite film with thin layer DNA on top was also investigated by the X-ray diffraction spectrometry (XRD) [Fig. 4(b)]. Three major diffraction peaks at 14.3°, 28.6° and 32.2° in $MAPbI_3$ perovskite films associating with (110), (220) and (310) planes [39], are all observed in the measured sample. Such result indicates that DNA doesn't influence the formation of orthorhombic structure of $MAPbI_3$, and thus ensuring the light response of the perovskite film.

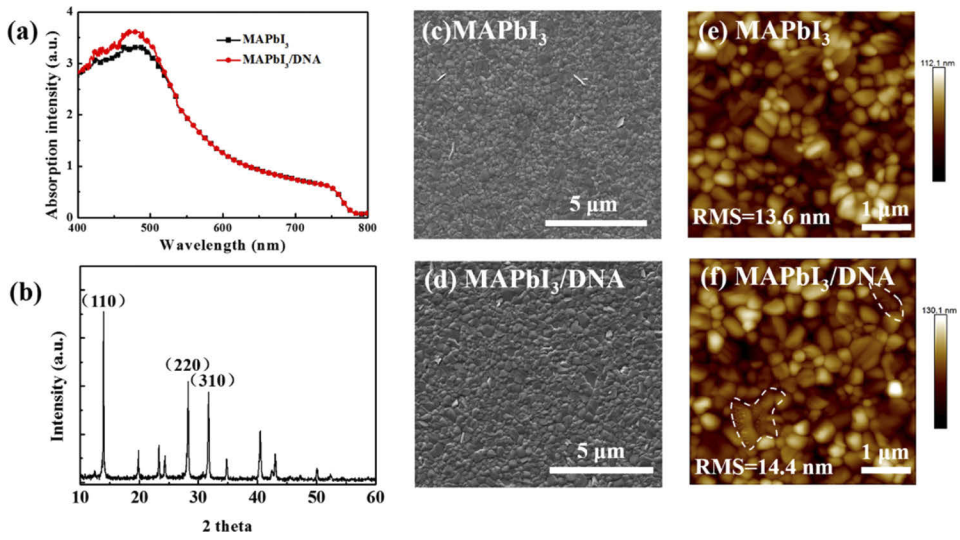

Fig. 4. (a) Absorption spectra of the perovskite films with and without DNA; (b) XRD of the perovskite film with DNA; SEM images a of perovskite film (c) with and (d) without DNA; AFM images of perovskite film (e) with and (f) without DNA. Here the DNA on the perovskite film was spin-coated in 1.5 wt. % solution.

Morphology study was conducted for the DNA coated perovskite film by top-view scanning electron microscopy (SEM), as shown in Figs. 4(c) and 4(d). The morphology of the perovskite film with and without DNA is almost the same, which can be explained by the film formation process as described in Methods. Since the DNA solution was spun after the perovskite film deposition, the morphology especially the grain sizes of the perovskite will not change. Furthermore, atomic force microscopy (AFM) was also conducted to characterize the surface roughness of the perovskite films with and without DNA [Figs. 4(e) and 4(f)]. The perovskite films with and without DNA all exhibit a smooth surface, revealing a root-mean-square (RMS) roughness of 14.4 nm and 13.6 nm, respectively, and the negligible change of RMS wouldn't influence the contact at interface between the perovskite film and the PCBM layer. The slightly rougher surface of the perovskite film with DNA is due to the aggregated DNA formed small bulge on the film surface, which is frame selected by white dotted line as shown in Fig. 4(f). Note, the DNA is not very soluble in CB, and the solution is more like a DNA dispersion in CB. Therefore, DNA did not form a very continuous film due to viscosity of the solution, rather than some island like features on the perovskites.

To get the deep insight into the reason of device performance improvement, the impedance spectroscopy (IS) measurement with transmission line model was employed and the corresponding results are shown in Fig. 5(a). Real impedances Z' of the PePDs with DNA decrease significantly, which is related to the increased I_{ph} [40]. In this circuit model, the constant phase element (CPE) indicates a non-ideal behavior of the capacitor, which is defined by two values, CPE-T and CPE-P. CPE-T is capacitance and CPE-P a non-homogeneity constant [41]. Compared with the reference device, CPE1-T of the PePDs with 1.5 wt.% DNA increases from 4.07×10^{-9} to 1.03×10^{-8} (Table 2), which indicates that DNA on the perovskite surface provides more potential pathways

Optical Materials EXPRESS

for electron transportation. R_3 in Fig. 5(a) corresponds to the perovskite film resistance, and the shunt pair R_2 and C_1 in represent two electrical contacts of the interfaces between the perovskite layer and electrodes [42]. R_3 for both PePDs with and without DNA is the same, indicating DNA has no influence on the resistance of the perovskite film. A high value of $R_2 = 4.33 \times 10^4$ Ω in the reference device indicates that the interface between the perovskite and the PCBM layer affect efficient charge carrier transportation, which can be proved by the low I_{ph} [38,39,43]. R_2 of the PePD with 1.5 wt.% DNA interfacial layer is much smaller (3.31×10^4 Ω), revealing that the loss due to interfacial resistance between the perovskite film and PCBM layer is minimized. Therefore, the DNA interfacial layer can act as electron extraction pathways, promotes the separation of photo-generated charge carrier and thus enhances the electron transport and I_{ph} [30–32] [Fig. 5(b)].

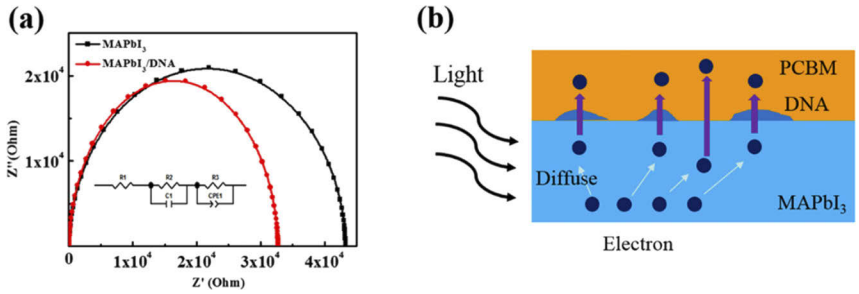

Fig. 5. (a) Impedance spectra of PePDs with and without DNA, inset shows the corresponding equivalent circuit; (b) Schematic diagram of the electron transport between $MAPbI_3$ and PCBM under light irradiation.

Table 2. Parameters of the equivalent circuit for PePDs with and without DNA

Device	R_1(Ω)	R_2(kΩ)	R_3(kΩ)	C_1(F)	CPE_1-T(F/cm^2)	CPE_1-P
Without DNA	34.7	43.3	1.5	1.52×10^{-9}	4.07×10^{-9}	0.91
With DNA	35.1	33.1	1.5	1.36×10^{-9}	1.03×10^{-8}	0.92

4. Conclusion

In summary, we for the first time introduced bio-materials DNA and guanine as functional interfacial layers in PePDs for photo sensitivity improvement. The results showed that the DNA interfacial layer on top of the perovskite films can act as electron extraction pathways, promote the separation of photo-generated charge carrier and thus facilitate the electron transport. As a result, the I_{ph} of the devices was significantly enhanced by nearly two times compared to the reference device without DNA. Moreover, with an optimized thickness of DNA, the PePD achieved a high D^* exceeding 10^{12} Jones over the wavelength region of 500-800 nm, and a maximum D^* of 1.85 $\times 10^{12}$ Jones at 745 nm at a bias of −0.2 V. This work expanded the application of bio-materials in perovskite devices and open a novel route to the future realization of ecofriendly and low-cost PePDs.

Funding

City University of Hong Kong (No. 9610423); State Scholarship Fund of China Scholarship Council (No. 201606070044); National Key R&D Program of China (2018YFB0407102); National Natural Science Foundation of China (51703019, 61421002, 61675041); Sichuan Province Science and Technology Support Program (2019YFG0121, 2019YFH0005, 2019YJ0178).

Optical Materials EXPRESS

References

1. W. Yang, J. Noh, N. Jeon, Y. Kim, S. Ryu, J. Seo, and S. Seok, "High-performance photovoltaic perovskite layers fabricated through intramolecular exchange," Science **348**(6240), 1234–1237 (2015).
2. M. Lee, J. Teuscher, T. Miyasaka, T. Murakami, and H. Snaith, "Efficient hybrid solar cells based on meso-superstructured organometal halide perovskites," Science **338**(6107), 643–647 (2012).
3. Y. Zheng, J. Kong, D. Huang, W. Shi, L. McMillon-Brown, H. E. Katz, J. Yu, and A. D. Taylor, "Spray coating of the PCBM electron transport layer significantly improves the efficiency of p-i-n planar perovskite solar cells," Nanoscale **10**(24), 11342–11348 (2018).
4. Y. Zheng, W. Shi, J. Kong, D. Huang, H. E. Katz, J. Yu, and A. D. Taylor, "A cytop insulating tunneling layer for efficient perovskite solar cells," Small Methods **1**(10), 1700244 (2017).
5. N. Wang, L. Cheng, R. Ge, S. Zhang, Y. Miao, W. Zou, C. Yi, Y. Sun, Y. Cao, R. Yang, Y. Wei, Q. Guo, Y. Ke, M. Yu, Y. Jin, Y. Liu, Q. Ding, D. Di, L. Yang, G. Xing, H. Tian, C. Jin, F. Gao, R. H. Friend, J. Wang, and W. Huang, "Perovskite light-emitting diodes based on solution-processed self-organized multiple quantum wells," Nat. Photonics **10**(11), 699–704 (2016).
6. Y. Shi, W. Wu, H. Dong, G. Li, K. Xi, G. Divitini, C. Ran, F. Yuan, M. Zhang, B. Jiao, X. Hou, and Z. Wu, "A strategy for architecture design of crystalline perovskite light-emitting diodes with high performance," Adv. Mater. **30**(25), 1800251 (2018).
7. Z. Wang, Z. Li, D. Zhou, and J. Yu, "Low turn-on voltage perovskite light-emitting diodes with methanol treated PEDOT: PSS as hole transport layer," Appl. Phys. Lett. **111**(23), 233304 (2017).
8. G. Xing, N. Mathews, S. S. Lim, N. Yantara, X. Liu, D. Sabba, M. Gratzel, S. Mhaisalkar, and T. C. Sum, "Low-temperature solution-processed wavelength-tunable perovskites for lasing," Nat. Mater. **13**(5), 476–480 (2014).
9. X. Yu, T. J. Marks, and A. Facchetti, "Metal oxides for optoelectronic applications," Nat. Mater. **15**(4), 383–396 (2016).
10. Z. Gu, K. Wang, W. Sun, J. Li, S. Liu, Q. Song, and S. Xiao, "Two-photon pumped $CH_3NH_3PbBr_3$ perovskite microwire lasers," Adv. Opt. Mater. **4**(3), 472–479 (2016).
11. Y. Dong, Y. Zou, J. Song, X. Song, and H. Zeng, "Recent progress of metal halide perovskite photodetectors," J. Mater. Chem. C **5**(44), 11369–11394 (2017).
12. X. Hu, X. Zhang, L. Liang, J. Bao, S. Li, W. Yang, and Y. Xie, "High-performance flexible broadband photodetector based on organolead halide perovskite," Adv. Funct. Mater. **24**(46), 7373–7380 (2014).
13. C. Xie and F. Yan, "Enhanced performance of perovskite/organic-semiconductor hybrid heterojunction photodetectors with the electron trapping effects," J. Mater. Chem. C **6**(6), 1338–1342 (2018).
14. M. Ahmadi, T. Wu, and B. Hu, "A review on organic-inorganic halide perovskite photodetectors: device engineering and fundamental physics," Adv. Mater. **29**(41), 1605242 (2017).
15. D. Zhao, J. Huang, R. Qin, G. Yang, and J. Yu, "Efficient visible-near-infrared hybrid perovskite:pbs quantum dot photodetectors fabricated using an antisolvent additive solution process," Adv. Opt. Mater. **6**(23), 1800979 (2018).
16. Y. Wei, Z. Ren, A. Zhang, P. Mao, H. Li, X. Zhong, W. Li, S. Yang, and J. Wang, "Hybrid organic/pbs quantum dot bilayer photodetector with low dark current and high detectivity," Adv. Funct. Mater. **28**(11), 1706690 (2018).
17. C. Ma, Y. Shi, W. Hu, M. H. Chiu, Z. Liu, A. Bera, F. Li, H. Wang, L. J. Li, and T. Wu, "Heterostructured WS_2 /$CH_3NH_3PbI_3$ photoconductors with suppressed dark current and enhanced photodetectivity," Adv. Mater. **28**(19), 3683–3689 (2016).
18. Z. Sun, L. Aigouy, and Z. Chen, "Plasmonic-enhanced perovskite-graphene hybrid photodetectors," Nanoscale **8**(14), 7377–7383 (2016).
19. D.-H. Kwak, D.-H. Lim, H.-S. Ra, P. Ramasamy, and J.-S. Lee, "High performance hybrid graphene-$CsPbBr_3$−xIx perovskite nanocrystal photodetector," RSC Adv. **6**(69), 65252–65256 (2016).
20. X. Zhuang, D. Zhang, X. Wang, X. Yu, and J. Yu, "Biocompatible and degradable gelatin dielectric based low-operating voltage organic transistors for ultra-high sensitivity NH_3 detection," Appl. Phys. Lett. **113**(26), 263301 (2018).
21. C. Liu, Q. Zhang, D. Wang, G. Zhao, X. Cai, L. Li, H. Ding, K. Zhang, H. Wang, D. Kong, L. Yin, L. Liu, G. Zou, L. Zhao, and X. Sheng, "High performance, biocompatible dielectric thin-film optical filters integrated with flexible substrates and microscale optoelectronic devices," Adv. Opt. Mater. **6**(15), 1800146 (2018).
22. X. Ning, X. Yu, H. Wang, R. Sun, R. E. Corman, H. Li, C. M. Lee, Y. Xue, A. Chempakasseril, Y. Yao, Z. Zhang, H. Luan, Z. Wang, W. Xia, X. Feng, R. H. Ewoldt, Y. Huang, Y. Zhang, and J. A. Rogers, "Mechanically active materials in three-dimensional mesostructures," Sci. Adv. **4**(9), eaat8313 (2018).
23. X. Yu, H. Wang, X. Ning, R. Sun, and J. A. Rogers, "Needle-shaped ultrathin piezoelectric microsystem for guided tissue targeting via mechanical sensing," Nat. Biomed. Eng. **2**(3), 165–172 (2018).
24. K. Liu, Z. Shi, S. Zhang, Z. Zhou, and T. H. Tao, "A silk cranial fixation system for neurosurgery," Adv. Healthcare Mater. **7**(6), 1701359 (2018).
25. W. Shi, J. Yu, W. Huang, and Y. Zheng, "Performance improvement of a pentacene organic field-effect transistor through a DNA interlayer," J. Phys. D: Appl. Phys. **47**(20), 205402 (2014).
26. K. J. Yu, D. Kuzum, S. W. Hwang, B. H. Kim, H. Juul, N. H. Kim, S. M. Won, K. Chiang, M. Trumpis, A. G. Richardson, H. Cheng, H. Fang, M. Thomson, H. Bink, D. Talos, K. J. Seo, H. N. Lee, S. K. Kang, J. H. Kim, J. Y. Lee, Y. Huang, F. E. Jensen, M. A. Dichter, T. H. Lucas, J. Viventi, B. Litt, and J. A. Rogers, "Bioresorbable silicon

Optical Materials EXPRESS

electronics for transient spatiotemporal mapping of electrical activity from the cerebral cortex," Nat. Mater. **15**(7), 782–791 (2016).
27. W. Shi, Y. Zheng, A. D. Taylor, J. Yu, and H. E. Katz, "Increased mobility and on/off ratio in organic field-effect transistors using low-cost guanine-pentacene multilayers," Appl. Phys. Lett. **111**(4), 043301 (2017).
28. P. Zalar, D. Kamkar, R. Naik, F. Ouchen, J. G. Grote, G. C. Bazan, and T. Q. Nguyen, "DNA electron injection interlayers for polymer light-emitting diodes," J. Am. Chem. Soc. **133**(29), 11010–11013 (2011).
29. A. Narazaki, A. Oyane, S. Komuro, R. Kurosaki, T. Kameyama, I. Sakamaki, H. Araki, and H. Miyaji, "Bioactive micropatterning of apatite immobilizing cell adhesion protein by laser-induced forward transfer with a shock absorber," Opt. Mater. Express **9**(7), 2807–2815 (2019).
30. C. V. Kumar, M. J. Novak, K. R. Benson, C. Baveghems, V. K. Thilakarathne, B. S. Stromer, and F. M. Ross, "Toward the design of bio-solar cells: high efficiency cascade energy transfer among four donor-acceptor dyes self-assembled in a highly ordered protein-DNA matrix," RSC Adv. **5**(88), 72416–72422 (2015).
31. W. Shi, X. Yu, Y. Zheng, and J. Yu, "DNA based chemical sensor for the detection of nitrogen dioxide enabled by organic field-effect transistor," Sens. Actuators, B **222**, 1003–1011 (2016).
32. J. Dagar, M. Scarselli, M. De Crescenzi, and T. M. Brown, "Solar cells incorporating water/alcohol-soluble electron-extracting DNA nanolayers," ACS Energy Lett. **1**(3), 510–515 (2016).
33. Y. Cho, J. Lee, J. Y. Lim, S. Yu, Y. Yi, and S. Im, "DNA-based small molecules for hole charge injection and channel passivation in organic heptazole field effect transistors," J. Phys. D: Appl. Phys. **50**(6), 065107 (2017).
34. S. Husaini, A. Lesko, E. M. Heckman, and R. G. Bedford, "Engineered bio-compatible graphene nanomaterials for nonlinear applications," Opt. Mater. Express **5**(1), 102–112 (2015).
35. M. Li, Y. Li, S. I. Sasaki, J. Song, C. Wang, H. Tamiaki, W. Tian, G. Chen, T. Miyasaka, and X. F. Wang, "Dopant-free zinc chlorophyll aggregates as an efficient biocompatible hole transporter for perovskite solar cells," ChemSusChem **9**(19), 2862–2869 (2016).
36. M. Li, S. I. Sasaki, Y. Sanehira, T. Miyasaka, H. Tamiaki, T. Ikeuchi, C. Gang, and X. F. Wang, "Biosupramolecular bacteriochlorin aggregates as hole-transporters for perovskite solar cells," J. Photochem. Photobiol., A **353**, 639–644 (2018).
37. H. Zhang, X. Wang, L. Yang, S. Zhang, Y. Zhang, C. He, W. Ma, and J. Hou, "Improved domain size and purity enables efficient all-small-molecule ternary solar cells," Adv. Mater. **29**(42), 1703777 (2017).
38. H. Wang, Y. Zheng, R. Qin, and J. Yu, "Highly sensitive panchromatic ternary polymer photodetectors enabled by Förster resonance energy transfer and post solvent treatment," J. Phys. D: Appl. Phys. **51**(10), 104002 (2018).
39. P. Fan, D. Zheng, Y. Zheng, and J. Yu, "Efficient and stable planar p-i-n perovskite solar cells by doping tungsten compound into PEDOT:PSS to facilitate perovskite crystalline," Electrochim. Acta **283**, 922–930 (2018).
40. E.-P. Yao, C.-C. Chen, J. Gao, Y. Liu, Q. Chen, M. Cai, W.-C. Hsu, Z. Hong, G. Li, and Y. Yang, "The study of solvent additive effects in efficient polymer photovoltaics via impedance spectroscopy," Sol. Energy Mater. Sol. Cells **130**, 20–26 (2014).
41. Y. Zheng, T. Goh, P. Fan, W. Shi, J. Yu, and A. D. Taylor, "Toward efficient thick active PTB7 photovoltaic layers using diphenyl ether as a solvent additive," ACS Appl. Mater. Interfaces **8**(24), 15724–15731 (2016).
42. W. Li, K. Hendriks, A. Furlan, W. Roelofs, M. Wienk, and A. Janssen, "Universal correlation between fibril width and quantum efficiency in diketopyrrolopyrrole-based polymer solar cells," J. Am. Chem. Soc. **135**(50), 18942–18948 (2013).
43. P. Fan, Y. Zheng, J. Song, and J. Yu, "N-type small molecule as an interfacial modification layer for efficient inverted polymer solar cells," Sol. Energy **158**, 278–284 (2017).

144.214.5.237 {ts '2019-09-06 22:19:16'}